Audio Engineering Society

Convention Paper 9938

Presented at the 144th Convention
2018 May 23 – 26, Milan, Italy

Continuous Measurement of Spatial Room Impulse Responses on a Sphere at Discrete Elevations

Nara Hahn and Sascha Spors

Institute of Communications Engineering, University of Rostock, Germany

Correspondence should be addressed to Nara Hahn (nara.hahn@uni-rostock.de)

ABSTRACT

In order to analyze a sound field with a high spatial resolution, a large number of measurements are required. A recently proposed continuous measurement technique is suited for this purpose, where the impulse response measurement is performed by using a moving microphone. In this paper, it is applied for the measurement of spatial room impulse responses on a spherical surface. The microphone captures the sound field on the sphere at discrete elevations while the system is periodically excited by the so-called perfect sequence. The captured signal is considered as a spatio-temporal sampling of the sound field, and the impulse responses are obtained by a spatial interpolation in the spherical harmonics domain. The elevation angles and the speed of the microphone are chosen is such a way that the spatial sampling points constitute a Gaussian sampling grid.

1 Introduction

The spatial structure of a sound field is of particular interest in the analysis and synthesis of a sound field [1, 2, 3]. In order to capture the spatio-temporal characteristics of a sound field, the impulse responses are measured at spatially distributed positions. The number of impulse responses, required to fully describe a sound field within a bounded region, is determined by the spatial bandwidth of the sound field [1, 2]. Conventionally, the spatial impulse responses are measured in a static experimental set-up, assuming linearity and time-invariance of the acoustic path.

Alternatively, a spatially dense measurement can be performed by using a continuously moving microphone. The microphone captures the sound field along a pre-defined trajectory while the system is periodically excited. The desired impulse responses are then extracted from the captured signal. Several approaches have been proposed to address the time-varying system identification problem [4, 5, 6, 7, 8]. In [7], it was pointed out that the continuous measurement can be considered as a sampling and reconstruction problem, and was proposed to perform the system identification by means of spatial interpolation. It was shown that currently available approaches can be also interpreted as spatial interpolation with different interpolation filters [9, 10]. In a series of studies, the continuous measurement on a circular path has been studied extensively [9, 11, 12, 13], where the anti-aliasing condition for the microphone speed is derived based on the bandwidth of the circular harmonics.

In this paper, an extension to the existing method is proposed for the impulse response measurement on a sphere. The measurement is composed of circular measurements at different elevation angles[1]. The trajectory of the microphone is determined by the spatial bandwidth of the sound field in the spherical harmonics domain. The number of elevation angles and the speed of the microphone is chosen in such a way that the distribution of the spatial sampling points constitutes a Gaussian sampling scheme. Since the discretized spherical harmonics expansion is known for Gaussian grids, the spatial interpolation in the spherical harmonics domain is straightforward.

Nomenclature and Mathematical Preliminaries

A sound field in the discrete-time domain is denoted by $p(\mathbf{r}, n)$, where $\mathbf{r}$ denotes the position vector and n the time index. Position vectors are represented in spherical coordinates $\mathbf{r} = (r, \theta, \phi)$,

$$\begin{aligned} x &= r \sin\theta \cos\phi \\ y &= r \sin\theta \sin\phi \\ z &= r \cos\theta, \end{aligned}$$

where r denotes the radius, $\theta \in [0, \pi]$ the colatitude angle, and $\phi \in [0, 2\pi)$ the azimuth angle. If there is no ambiguity from the context, a point on a sphere is denoted by (θ, ϕ) for brevity. The sampling frequency is denoted by f_s and the speed of sound by c.

A sound field on a sphere of radius R can be represented as a spherical harmonics expansion [16, (6.48)],

$$p(\theta, \phi, n) = \sum_{\nu=0}^{\infty} \sum_{\mu=-\nu}^{\nu} \breve{p}_{\nu\mu}(n) Y_{\nu\mu}(\theta, \phi), \quad (1)$$

where $Y_{\nu\mu}(\theta, \phi)$ denotes the spherical harmonic, and $\breve{p}_{\nu\mu}(n)$ the expansion coefficient of degree ν and order μ. The spherical harmonic is defined as [16, (6.20)]

$$Y_{\nu\mu}(\theta, \phi) \equiv \sqrt{\frac{2\nu+1}{4\pi} \frac{(\nu-\mu)!}{(\nu+\mu)!}} \mathcal{P}_\nu^\mu(\cos\theta) e^{i\mu\phi}, \quad (2)$$

with $\mathcal{P}_\nu^\mu(\cdot)$ denoting the corresponding associated Legendre function. The expansion coefficient can be considered as a projection of the function onto the respective spherical harmonic, which is given as a surface integral [16, (6.49)],

$$\breve{p}_{\nu\mu}(n) = \int_0^{2\pi} \int_0^{\pi} p(\theta, \phi, n) Y_{\nu\mu}^*(\theta, \phi) \sin\theta \mathrm{d}\theta \mathrm{d}\phi, \quad (3)$$

where $(\cdot)^*$ denotes the conjugate complex. Equation (3) and (1) constitute the forward and inverse spherical harmonic transform, respectively.

In practice, only a finite number of measurements are available, therefore, the spherical harmonics transform (3) has to be discretized. To avoid spatial aliasing, the bandwidth of $\breve{p}_{\nu\mu}(n)$ in the spherical harmonics domain has to be taken into account. Although a sound field on a sphere is not strictly band-limited, it was shown in [17, 18] that a homogeneous sound field within a source-free region can be reasonably approximated by a truncated spherical harmonics expansion. The maximum harmonic order of the truncated expansion is referred to as the spatial bandwidth and can be approximated as [18, Sec. E]

$$\mathcal{M}_\eta = \left\lceil \frac{e\pi f R}{c} \right\rceil + \eta, \quad (4)$$

where $\lceil \cdot \rceil$ denotes the ceiling function, f the temporal frequency, and η a non-negative integer. Since the truncation error decreases exponentially with increasing η [17, 18], larger η leads to a more pessimistic (broader) bandwidth. For broadband signals, $\mathcal{M}_\eta$ is computed by substituting f with the temporal bandwidth.

2 Continuous Measurement

In the first part of this section, the continuous measurement technique based on spatial interpolation is introduced. As proposed in [7, 11], the time-varying system identification is treated as a sampling and reconstruction problem. From Sec. 2.6 on, the method is extended to the measurement of impulse responses on an open sphere, where the measurement is performed at multiple elevation angles.

[1] A similar configuration was considered in [14, 15] for head-related impulse responses, where the loudspeakers are arranged at discrete elevations and a head-and-torso simulator was continuously rotated.

2.1 System Model

It is assumed that the acoustic transmission from a source to a receiver is characterized by a finite impulse response (FIR) model. A sound field on a spherical surface $r = R$ thus reads

$$p(\theta, \phi, n) = \sum_{k=0}^{N_h-1} \psi(n-k)\ h(\theta, \phi, k), \qquad (5)$$

where $h(\theta, \phi, n)$ denotes the impulse response, $\psi(n)$ the source signal, and N_h the length of $h(\theta, \phi, n)$. The source position, $\mathbf{r}_\mathrm{s} = (R_\mathrm{s}, \theta_\mathrm{s}, \phi_\mathrm{s})$ with $R_\mathrm{s} > R$, is omitted for brevity.

2.2 Excitation by Perfect Sequence

For a continuous measurement, the system is excited by a periodic signal $\psi(n+N) = \psi(n)$ that exhibits self-orthogonality,

$$\sum_{k=0}^{N-1} \psi(k)\ \psi(n-k) = \sigma_\psi^2 \cdot \delta_{n \bmod N}, \qquad (6)$$

where $n \bmod N$ denotes n modulo N, $\sigma_\psi^2 \equiv \sum_{k=0}^{N-1} \psi(k)^2$ the energy of $\psi(n)$ within a period, and δ_n the shorthand for the Kronecker delta δ_{n0}. Equation (6) states that the circular autocorrelation of the signal is an impulse train. A signal satisfying (6) is called a perfect sequence [19]. Well-known examples are the maximum length sequence (MLS) and the perfect sweep [20]. In the remainder, the excitation period N is assumed to be longer than N_h so that the identified impulse responses do not suffer from temporal aliasing [5]. Also, $\sigma_\psi = 1$ is assumed for convenience.

Once the system is excited by $\psi(n)$, the sound field $p(\theta, \phi, n)$ has the same N-periodicity. The impulse response at a given position can be obtained by computing the length-N circular cross-correlation of $p(\theta, \phi, n)$ and $\psi(n)$,

$$h(\theta, \phi, n) = \sum_{k=0}^{N-1} p(\theta, \phi, k)\ \psi(k-n), \qquad (7)$$

which can be proven by inserting (5) into (7) and exploiting (6). Note from (7) that the computation of $h(\theta, \phi, n)$ requires N consecutive samples of $p(\theta, \phi, n)$. This implies that the sound field at a particular position has to be captured at least for one period, in order to obtain the impulse response.

2.3 Spatial Sampling

Let assume that an omni-directional microphone moves on a spherical trajectory represented by $\mathbf{r}'(n) = \big(R, \vartheta(n), \varphi(n)\big)$ and captures the sound field. If the spatial averaging effect on the diaphragm due to the movement is neglected, the captured signal $s(n)$ represents the sound field at the instantaneous positions,

$$\begin{aligned} s(n) &= p\big(\vartheta(n), \varphi(n), n\big) \\ &= p\big(\vartheta(n), \varphi(n), n \bmod N\big), \end{aligned} \qquad (8)$$

where the second equality is due to above discussed periodicity. The impulse responses cannot be computed by using (7) at this point, since only one sample is available for each position.

To better understand the properties of the captured signal, the samples of $s(n)$ are grouped into N disjoint sets,

$$\begin{aligned} \mathcal{S}_m &= \Big\{ s(m), s(m+N), s(m+2N), \dots \Big\} \qquad (9) \\ &= \Big\{ p\big(\vartheta(m), \varphi(m), m\big), \\ &\quad\ p\big(\vartheta(m+N), \varphi(m+N), m\big), \\ &\quad\ p\big(\vartheta(m+2N), \varphi(m+2N), m\big), \dots \Big\}, \end{aligned}$$

for $m = 0, 1, \dots, N-1$. The elements of $\mathcal{S}_m$ can be considered as the sound field at the same moment $p(\theta, \phi, n)|_{n=m}$ but captured at different positions,

$$\begin{gathered} \big(\vartheta(m), \varphi(n)\big), \\ \big(\vartheta(m+N), \varphi(m+N)\big), \\ \big(\vartheta(m+2N), \varphi(m+2N)\big), \\ \vdots \end{gathered} \qquad (10)$$

The captured signal thus can be considered as a spatio-temporal sampling of $p(\theta, \phi, n)$.

2.4 Spatial Interpolation

In order to compute the impulse response at a position, the corresponding sound field has to be reconstructed from the spatial samples. The sound

field at the target position is estimated by means of interpolation,

$$\hat{p}(\theta,\phi,n)|_{n=m} = \sum_l \alpha_l \; p(\vartheta_{m+lN}, \varphi_{m+lN}, m) = \sum_l \alpha_l \; s(m+lN), \tag{11}$$

for $m = 0, 1, \ldots, N-1$. The hat $\hat{(\cdot)}$ denotes the estimate of the argument and α_l the interpolation weight. The interpolation has to be performed independently for each m, since the sampling positions (10) exhibit different spatial distributions. Once the sound field is reconstructed for all $m = 0, \ldots, N-1$, the impulse response $\hat{h}(\theta,\phi,n)$ is computed by substituting $p(\theta,\phi,n)$ with $\hat{p}(\theta,\phi,n)$ in (7),

$$\hat{h}(\theta,\phi,n) = \sum_{k=0}^{N-1} \hat{p}(\theta,\phi,k) \; \psi(k-n), \tag{12}$$

for $n = 0, 1, \ldots, N-1$.

An important prerequisite of the presented approach is that the sampling points in (10) perform an aliasing-free discretization of the sound field. The problem of distributing multiple points on a sphere has been extensively studies in the context of spherical microphone/loudspeaker arrays and various types of distributions have been proposed and analyzed [21, 22, 23]. Among others, the Gaussian sampling scheme is considered in this paper for the continuous measurement, which is briefly introduced in the following.

2.5 Gaussian Sampling

In the Gaussian sampling, a sound field with a spatial bandwidth of $\mathcal{M}$ is sampled at $2(\mathcal{M}+1)^2$ points on the sphere [1, Sec. 3.3],

$$(\theta_\zeta, \phi_\xi), \quad \text{for } \zeta = 0, 1, \ldots, \mathcal{M} \quad \xi = 0, 1, \ldots, 2\mathcal{M}+1. \tag{13}$$

While the azimuth angles ϕ_ξ are equally spaced in $[0, 2\pi)$,

$$\phi_\xi = \frac{2\pi}{2(\mathcal{M}+1)}\xi + \Delta, \quad \xi = 0, \ldots, 2\mathcal{M}+1, \tag{14}$$

whereas the colatitude angles θ_ζ are given as the zeros of the Legendre polynomial [1, (3.20)],

$$\mathcal{P}_{\mathcal{M}+1}(\cos\theta_\zeta) = 0, \quad \zeta = 0, \ldots, \mathcal{M}. \tag{15}$$

Note that, in (14), a circular shift Δ can be applied to the azimuth angles without affecting the properties of Gaussian sampling scheme.

Once a sound field of order $\mathcal{M}$ is sampled with a Gaussian grid, the discretized spherical harmonics can be computed as [1, (3.22)],

$$\breve{p}_{\nu\mu}(n) = \sum_{\zeta=0}^{\mathcal{M}} \sum_{\xi=0}^{2\mathcal{M}+1} p(\theta_\zeta, \phi_\xi, n) \times w_\zeta \; Y^*_{\nu\mu}(\theta_\zeta, \phi_\xi), \tag{16}$$

for $\nu \leq \mathcal{M}$ and $|\mu| \leq \nu$. The quadrature weight w_ζ is given as [1, (3.21)]

$$w_\zeta = \frac{\pi}{\mathcal{M}+1} \frac{2(1-\cos^2\theta_\zeta)}{(\mathcal{M}+2)^2 \mathcal{P}^2_{\mathcal{M}+2}(\cos\theta_\zeta)}, \tag{17}$$

which assures the orthogonality of the space-discrete spherical harmonic transform.

2.6 Trajectories at Discrete Elevations

For the continuous measurement on a sphere, the microphone is moved in such a way that the sampling points of each $\mathcal{S}_m$ in (9) constitute a Gaussian sampling gird. As depicted in Fig. 1, the measurement is performed for $\mathcal{M}+1$ different elevations, where the colatitude angles are given by (15). The ζ-th trajectory is denoted by

$$\mathbf{r}'_\zeta = \big(\vartheta_\zeta, \varphi_\zeta(n)\big), \tag{18}$$

for $\zeta = 0, \ldots, \mathcal{M}$, where the time argument for ϑ_ζ is omitted because the elevation angle is fixed for each trajectory. The respective captured signal is denoted by $s_\zeta(n)$.

The number of samples in the azimuth angle is determined by the angular speed of the microphone. As uniform sampling is required, the microphone is moved at a constant angular speed Ω (in rad/s). The azimuthal position thus reads

$$\varphi(n) = \frac{\Omega \times n}{f_s}. \tag{19}$$

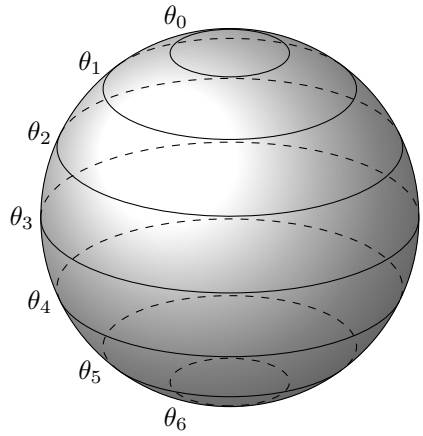

Fig. 1: Microphone trajectories with discrete elevations. The colatitude angles θ_ζ satisfy (15) for $\mathcal{M} = 6$.

where the subscript ζ is dropped as the azimuthal sampling is chosen identical for all elevations.

The length of the captured signal $s(n)$ is $\frac{2\pi f_s}{\Omega}$ samples, whereas the number of samples in each $\mathcal{S}_m$ is reduced by a factor of N,

$$\frac{1}{N} \times \frac{2\pi f_s}{\Omega}. \tag{20}$$

By equating (20) with $2(\mathcal{M}+1)$, the angular speed is obtained,

$$\Omega = \frac{\pi f_s}{(\mathcal{M}+1)N}. \tag{21}$$

This can be considered as the anti-aliasing condition for the continuous measurement. The higher the spatial bandwidth, the slower the microphone has to move. Note that (21) holds only for the particular measurement set-up considered here, where the sampling points are matched to the Gaussian grid.

As a result, the sound field $p(\theta, \phi, n)|_{n=m}$ is sampled at discrete positions,

$$\big(\vartheta_\zeta, \varphi(m + \xi N)\big), \tag{22}$$

for $\zeta = 0, 1, \ldots, \mathcal{M}$ and $\xi = 0, 1, \ldots, 2(\mathcal{M}+1)$. The distribution (22) differs for each m, as the azimuth angles are shifted by $\frac{\Omega \times m}{f_s}$.

2.7 Spherical Harmonics Interpolation

The spatial interpolation is performed in the spherical harmonics domain as follows. Based on the sampled sound field of the previous section, the spherical harmonics expansion coefficients are computed up to a given order $\mathcal{M}$ by using (16),

$$\breve{p}_{\nu\mu}(m) = \sum_{\zeta=0}^{\mathcal{M}} \sum_{\xi=0}^{2\mathcal{M}+1} p\left(\vartheta_\zeta, \varphi(m+\xi N), m\right) \times w_\zeta Y^*_{\nu\mu}\big(\vartheta_\zeta, \varphi(m+\xi N)\big) \tag{23}$$

$$= \sum_{\zeta=0}^{\mathcal{M}} \sum_{\xi=0}^{2\mathcal{M}+1} s_\zeta(m+\xi N) \times w_\zeta Y^*_{\nu\mu}\big(\vartheta_\zeta, \varphi(m+\xi N)\big), \tag{24}$$

for $m = 0, \ldots, N-1$. Equation (24) shows how the samples of the captured sound field are used in the computation. The sound field at a desired position is then computed as a spherical harmonics expansion (1) with the same harmonic order,

$$\hat{p}(\theta, \phi, m) = \sum_{\nu=0}^{\mathcal{M}} \sum_{\mu=-\nu}^{\nu} \breve{p}_{\nu\mu}(m) Y_{\nu\mu}(\theta, \phi). \tag{25}$$

Finally, the impulse response at the corresponding position is obtained,

$$\hat{h}(\theta, \phi, n) = \sum_{k=0}^{N-1} \hat{p}(\theta, \phi, k)\psi(k-n). \tag{26}$$

The above process can be considered as an 2-dimensional interpolation on a sphere,

$$\hat{p}(\theta, \phi, n)|_{n=m} = \sum_{\zeta=0}^{\mathcal{M}} \sum_{\xi=0}^{2\mathcal{M}+1} \alpha^m_{\zeta\xi} \times p\big(\vartheta_\zeta, \varphi(m+\xi N), m\big). \tag{27}$$

The interpolation weight $\alpha^m_{\zeta\xi}$ can be derived by substituting (23) into (25),

$$\begin{aligned}\alpha^m_{\zeta\xi} =& w_\zeta \sum_{\nu=0}^{\mathcal{M}} \sum_{\mu=-\nu}^{\nu} Y_{\nu\mu}(\theta, \phi) Y^*_{\nu\mu}\big(\vartheta_\zeta, \varphi(m+\xi N)\big) \\ =& w_\zeta \frac{\mathcal{M}+1}{4\pi(\cos\Theta^m_{\zeta\xi} - 1)} \\ & \times \Big[\mathcal{P}_{\mathcal{M}+1}(\cos\Theta^m_{\zeta\xi}) - \mathcal{P}_{\mathcal{M}}(\cos\Theta^m_{\zeta\xi})\Big],\end{aligned} \tag{28}$$

where $\Theta^m_{\zeta\xi}$ denotes the angle between (θ, ϕ) and $\big(\vartheta_\zeta, \varphi(m+\xi N)\big)$.

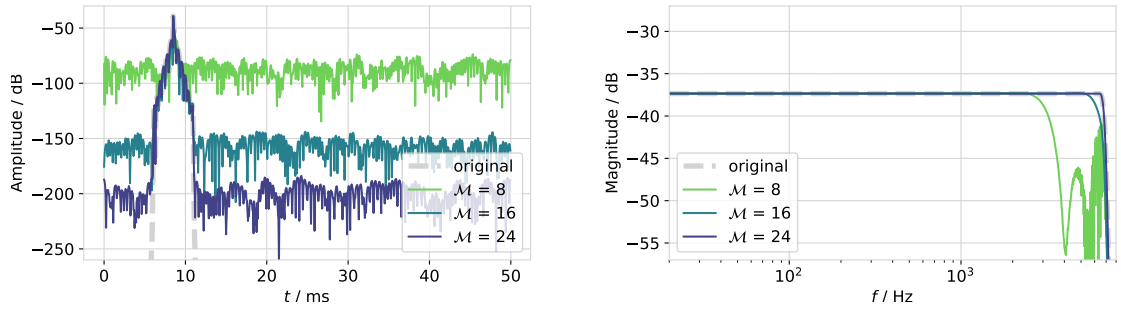

(a) Impulse responses **(b)** Transfer functions

Fig. 2: Impulse responses and transfer functions for $(\theta, \phi) = (62.0°, 165.9°)$.

3 Evaluation

The presented method is evaluated by numerical simulations, where the spatial impulse responses on an open sphere of radius $R = 0.15$ m are measured by using a moving microphone. A point source is placed at $\mathbf{r}_\mathrm{s} = (3, \frac{\pi}{4}, \frac{\pi}{2})$ in the free field. In the continuous-time domain, the impulse responses thus reads

$$h(\theta, \phi, t) = \frac{1}{4\pi} \frac{\delta\left(t - \frac{\rho(\mathbf{r}_\mathrm{s}, \mathbf{r})}{c}\right)}{\rho(\mathbf{r}_\mathrm{s}, \mathbf{r})}. \tag{29}$$

Here, $\delta(\cdot)$ denotes the Dirac delta function, and $\rho(\mathbf{r}_\mathrm{s}, \mathbf{r})$ the Euclidean distance,

$$\begin{aligned} \rho(\mathbf{r}_\mathrm{s}, \mathbf{r}) \equiv \|(&R \sin\theta \cos\phi - r_\mathrm{s} \sin\theta_\mathrm{s} \cos\phi_\mathrm{s}, \\ &R \sin\theta \sin\phi - r_\mathrm{s} \sin\theta_\mathrm{s} \sin\phi_\mathrm{s}, \\ &R \cos\theta - r_\mathrm{s} \cos\theta_\mathrm{s})\|, \end{aligned} \tag{30}$$

where $\|\cdot\|$ denotes the Euclidean norm. As the propagation delay $\rho(\mathbf{r}_\mathrm{s}, \mathbf{r})/c$ is generally not an integer multiple of $\frac{1}{f_s}$, Lagrange filters of order 23 are used for fractional delay interpolation [24]. The fractional delay filter coefficients are computed at a sampling frequency of 32 kHz, and converted back to the original sampling rate of $f_s = 16$ kHz. The impulses are low-pass filtered with a cut-off frequency of 6.4 kHz. The speed of sound is set to $c = 343$ m/s.

The point source is driven by a perfect sequence of length $N = 800$ (50 ms) which exhibits a unit magnitude and a random phase in the frequency domain. According to (4), the spatial bandwidth of the spatial impulse response is $\mathcal{M}_0 = 24$. For $\mathcal{M}_0$, the corresponding angular speed is $\Omega = \frac{\pi f_s}{(\mathcal{M}_0+1)N} \approx 2.51$ rad/s which is obtained by (21).

An omnidirectional microphone is used for the continuous measurement. The measurements are performed for varying spatial bandwidth $\mathcal{M}$ ranging from 2 to 36. For a given $\mathcal{M}$, the elevation angles and the speed of the microphone are determined by (15) and (21), respectively. Therefore, the sound field is sampled at a Gaussian grid in all cases. The microphone is moved counter-clockwise on the circular paths at different elevations.

By using the proposed method, 5202 impulse responses on a Gaussian grid of order $\mathcal{M} = 50$ are obtained (51 elevations and 102 azimuths). The spherical harmonics interpolation is performed by using the Sound Field Analysis Toolbox[2]. Individual impulse responses at a selected position $(62.0°, 165.9°)$ and the corresponding transfer functions are shown in Fig. 2. Figure 2(a) shows that the noise floor gets lower for higher spatial bandwidth $\mathcal{M}$. The fine structure of the impulse is more accurately identified for higher $\mathcal{M}$, which can be also confirmed by the magnitude response at high frequencies shown in Fig. 2(b). If the anti-aliasing condition is not fulfilled, high frequency components are affected by spatial aliasing.

The performance of the individual impulse responses are evaluated in terms of the normalized

[2] https://github.com/spatialaudio/sfa-numpy

mean square error (NMSE),

$$\mathcal{E}(\theta,\phi) = \left[\frac{\sum_{n=0}^{N-1} \left| h(\theta,\phi) - \hat{h}(\theta,\phi) \right|^2}{\sum_{n=0}^{N-1} \left| h(\theta,\phi) \right|^2} \right]^{1/2} . \quad (31)$$

The NMSEs for different measurement set-ups are shown in Fig. 3. The direction of the source $(\theta_\mathrm{s}, \phi_\mathrm{s})$ is indicated by $\times$. As expected, higher accuracy is achieved for higher-order sampling schemes (more elevations and slower microphone movement). Although the anti-aliasing condition (21) is already fulfilled in Fig. 3(b), the performance is further improved in Fig. 3(c). This is due to the approximation of the spatial bandwidth used in the derivation.

In order to compare the overall performance of different measurement sets, the NMSE is averaged over the sphere. The mean NMSE, denoted by $\bar{\mathcal{E}}$, is computed as the spherical harmonics coefficient of degree 0 and order 0,

$$\bar{\mathcal{E}} = \frac{\breve{\mathcal{E}}_{00}}{\sqrt{4\pi}}, \quad (32)$$

where $1/\sqrt{4\pi}$ is the normalization factor. The average NMSE for different $\mathcal{M}$ is shown in Fig. 4 together with the anti-aliasing condition indicated by the vertical dashed line. Satisfying the anti-aliasing condition achieves a mean NMSE of -60 dB. If higher accuracy is required, a more pessimistic approximation of the spatial bandwidth has to be considered, i.e. larger η in (4).

The simulation results show that the presented method is able to measure the spatial impulse responses with reasonable accuracy, if the anti-aliasing condition is fulfilled. The impulse responses can be further used for sound field analysis and multichannel sound reproduction. It is worth noting that the continuous measurement using an omnidirectional microphone exhibits the same numerical properties, e.g. forbidden frequencies, as conventional spherical measurements [1, Sec. 4.1]. The latter can be, of course, avoided by using a rigid sphere or cardioid microphones [1, Sec. 4.2 and 4.3].

4 Conclusion

The continuous measurement technique previously proposed by the authors is extended to spherical measurements. The measurement is performed at discrete elevation angles where the microphone moves at a constant speed. In order to mimic a Gaussian sampling scheme, the elevation angles and the speed of the microphone are selected based on the spatial bandwidth of the sound field under consideration. The performance of the presented approach is demonstrated by numerical simula-

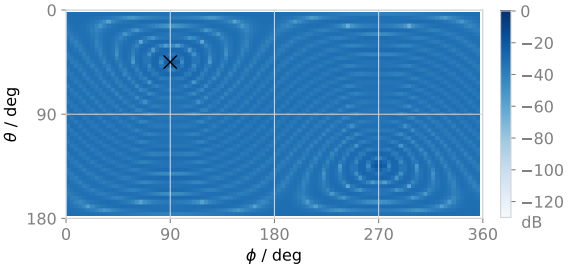

(a) $\mathcal{M} = 20$ ($\bar{\mathcal{E}} = -34$ dB)

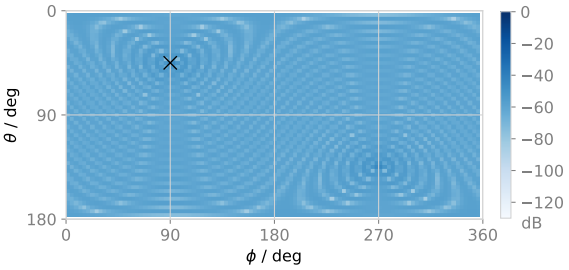

(b) $\mathcal{M} = 24$ ($\bar{\mathcal{E}} = -60$ dB)

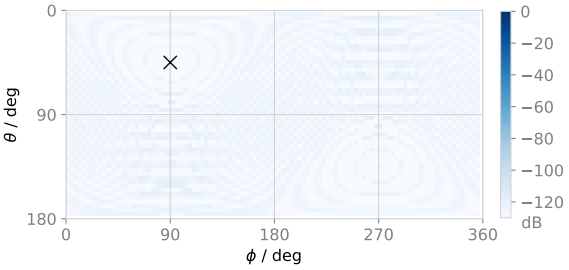

(c) $\mathcal{M} = 36$ ($\bar{\mathcal{E}} = -126$ dB)

Fig. 3: NMSE of the individual impulse responses for different Gaussian sampling orders $\mathcal{M}$.

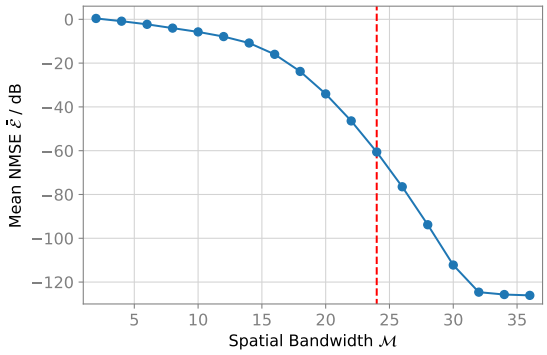

Fig. 4: Mean NMSE for varying spatial bandwidths. The vertical dashed line indicates the approximated spatial bandwidth $\mathcal{M}_0$ of the sound field in (4).

tions. The results validate the interpretation of the continuous measurement as a sampling and reconstruction problem.

The presented method can be easily employed in a motorized measurement system, since the microphone has to be rotated only in the azimuth direction. The present study is designed as a proof of concept, therefore has to be further investigated in real measurements.

Acknowledgment

This research was supported by a grant of the Deutsche Forschungsgemeinschaft (DFG) SP 1295/7-1.

References

[1] Rafaely, B., *Fundamentals of Spherical Array Processing*, Springer, 2015.

[2] Kuntz, A., *Wave Field Analysis using Virtual Circular Microphone Arrays*, Verlag Dr. Hut, 2008.

[3] Spors, S., Wierstorf, H., Raake, A., Melchior, F., Frank, M., and Zotter, F., "Spatial Sound with Loudspeakers and its Perception: A Review of the Current State," *IEEE Proc.*, 101(9), pp. 1920–1938, 2013.

[4] Ajdler, T., Sbaiz, L., and Vetterli, M., "Dynamic Measurement of Room Impulse Responses Using a Moving Microphone," *J. Acoust. Soc. Am. (JASA)*, 122(3), pp. 1636–1645, 2007.

[5] Antweiler, C. and Enzner, G., "Perfect Sequence LMS for Rapid Acquisition of Continuous-azimuth Head Related Impulse Responses," in *Proc. IEEE Workshop Appl. Signal Process. Audio Acoust. (WASPAA)*, pp. 281–284, New Paltz, NY, USA, 2009.

[6] Hulsebos, E. M., *Auralization using Wave Field Synthesis*, Ph.D. thesis, Delft University of Technology, Delft, The Netherlands, 2004.

[7] Hahn, N. and Spors, S., "Identification of Dynamic Acoustic Systems by Orthogonal Expansion of Time-variant Impulse Responses," in *Proc. 6th Int. Symp. Commun. Control Signal Process. (ISCCSP)*, Athens, Greek, 2014.

[8] Katzberg, F., Mazur, R., Maass, M., Koch, P., and Mertins, A., "Measurement of Sound Fields Using Moving Microphones," in *Proc. IEEE Int. Conf. Acoust. Speech Signal Process. (ICASSP)*, New Orleans, USA, 2017.

[9] Hahn, N. and Spors, S., "Comparison of Continuous Measurement Techniques for Spatial Room Impulse Responses," in *Proc. Eur. Signal Process. Conf. (EUSIPCO)*, Budapest, Hungary, 2016.

[10] Hahn, N. and Spors, S., "Analysis of Time-Varying System Identification Using Normalized Least Mean Square (NLMS) in the Context of Data-Based Binaural Synthesis," in *Proc. 42nd German Annu. Conf. Acoust. (DAGA)*, Aachen, Germany, 2016.

[11] Hahn, N. and Spors, S., "Continuous Measurement of Impulse Responses on a Circle Using a Uniformly Moving Microphone," in *Proc. Eur. Signal Process. Conf. (EUSIPCO)*, Nice, France, 2015.

[12] Hahn, N. and Spors, S., "Spatial Aliasing in Continuous Measurement of Spatial Room Impulse Responses," in *Proc. 43rd German*

Annu. Conf. Acoust. (DAGA), Kiel, Germany, 2017.

[13] Hahn, N. and Spors, S., "Continuous Measurement of Spatial Room Impulse Responses Using a Non-Uniformly Moving Microphone," in *Proc. IEEE Workshop Appl. Signal Process. Audio Acoust. (WASPAA)*, New Paltz, NY, USA, 2017.

[14] Enzner, G., "3D-Continuous-Azimuth Acquisition of Head-Related Impulse Responses Using Multi-Channel Adaptive Filtering," in *Proc. IEEE Workshop Appl. Signal Process. Audio Acoust. (WASPAA)*, pp. 325–328, IEEE, 2009.

[15] Richter, J. and Fels, J., "On the Influence of Continuous Subject Rotation during HRTF Measurements," *The J. Acoust. Soc. Am. (JASA)*, 141(5), pp. 3986–3986, 2017.

[16] Williams, E. G., *Fourier Acoustics: Sound Radiation and Nearfield Acoustical Holography*, Academic press, 1999.

[17] Abhayapala, T. D., Pollock, T. S., and Kennedy, R. A., "Characterization of 3D Spatial Wireless Channels," in *Proc. IEEE 58th Vehicular Technol. Conf. (VTC)*, volume 1, pp. 123–127, IEEE, 2003.

[18] Kennedy, R. A., Sadeghi, P., Abhayapala, T. D., and Jones, H. M., "Intrinsic Limits of Dimensionality and Richness in Random Multipath Fields," *IEEE Trans. Signal Process.*, 55(6), pp. 2542–2556, 2007.

[19] Lüke, H. D., *Korrelatioknssignale*, Springer, 1992.

[20] Aoshima, N., "Computer-generated Pulse Signal Applied for Sound Measurement," *J. Acoust. Soc. Am. (JASA)*, 69(5), pp. 1484–1488, 1981.

[21] Rafaely, B., "Analysis and Design of Spherical Microphone Arrays," *IEEE Trans. Speech Audio process.*, 13(1), pp. 135–143, 2005.

[22] Rafaely, B., Weiss, B., and Bachmat, E., "Spatial Aliasing in Spherical Microphone Arrays," *IEEE Trans. Signal Process.*, 55(3), pp. 1003–1010, 2007.

[23] Zotter, F., "Sampling Strategies for Acoustic Holography/Holophony on the Sphere," in *Proc. NAG-DAGA Int. Conf. Acoust.*, pp. 1–4, Rotterdam, The Netherlands, 2009.

[24] Laakso, T. I., Valimaki, V., Karjalainen, M., and Laine, U. K., "Splitting the Unit Delay," *IEEE Signal Process. Mag.*, 13(1), pp. 30—-60, 1996.